

Barotropic Instability of the Polar Night Jet Stream¹

DENNIS L. HARTMANN

Department of Atmospheric Sciences, University of Washington, Seattle, Washington 98195

(Manuscript received 23 August 1982, in final form 15 November 1982)

ABSTRACT

An eigenvalue analysis of the nondivergent barotropic model on a sphere and an initial value analysis of a baroclinic, quasi-geostrophic model on a sphere are used to study barotropically unstable zonal flows similar to those observed in the wintertime stratosphere. The unstable modes fall into two categories. Polar modes associated with regions of negative potential vorticity gradient on the polar flank of the stratospheric westerly jet are most unstable for zonal wavenumbers 1 and 2 which have significant growth rates and have periods on the order of 3–4 days and 1.5–2 days, respectively. These polar modes correspond to a wave observed by Venne and Stanford (1982). Mid-latitude modes associated with regions of negative potential vorticity gradient on the equatorward flank of the stratospheric westerly jet have much longer periods. For wind profiles near marginal stability the most unstable modes occur for the lowest zonal wavenumbers 1–3 and have periods which are on the order of a week or more for wavenumbers 1 and 2. It is suggested that these instabilities may interact strongly with planetary waves propagating upward from the troposphere producing an additional *in situ* source of energy for these waves.

1. Introduction

A widely held perception of the upper stratosphere and mesosphere is that they are regions whose large-scale dynamics are dominated by slowly varying planetary waves propagating upward from below. There is mounting evidence, however, that while this view may be a reasonable first approximation, there is really much more of interest and importance taking place in these regions. Rocket data taken at frequent intervals suggest the presence of very large amplitude disturbances of less than planetary scale and with periods on the order of a few days or less (e.g., Leovy and Ackerman, 1973).

Recent analyses of satellite radiance data by Venne and Stanford (1979, 1982) (hereafter VS) have indicated the presence of a rapidly eastward moving component of zonal wavenumber 1 near the polar stratopause during winter. This component, which VS have called the 4-day wave, is evidenced by a broad maximum in the eastward moving variance of wavenumber 1 which extends between periods of ~3–5 days and between latitudes of about 50°–90°. The peak variance during Southern Hemisphere winter occurs at a period of about 3.5 days and at about 70°S. This wave is clearly defined in the Southern Hemisphere, but there is also evidence of it in the Northern Hemisphere. The amplitude of the 4-day

wave increases more rapidly with height between 50 and 4 mb than a wave of constant energy density and the phase is constant with height, suggesting an *in situ* source for the wave. According to the results of VS the wave has a north–south phase variation which indicates an equatorward momentum flux in the region poleward of the jet in the Southern Hemisphere, but a poleward flux in the Northern Hemisphere.

Leovy and Webster (1976) observed that zonal mean wind distributions often had regions of negative mean vorticity gradient that resulted from strong meridional wind curvature, and questioned whether barotropic instability might be an important process in the upper stratosphere. Pfister (1979) has recently investigated the potential importance of barotropic instability near the stratopause. Using a β -plane analysis he found significant growth rates for zonal wavenumbers greater than 4 for wind profiles similar to those observed on particular days. He also found that realistic vertical shear tended to decrease the growth rates of modes resulting from mostly barotropic instabilities.

In this paper we will point out that barotropic instability resulting from regions of negative potential vorticity gradient on the poleward side of the polar night jet can produce a wave of the “4-day” variety as described by VS. Perhaps more importantly, waves growing on negative potential vorticity gradients on the equatorward side of the polar night jet will tend to be of planetary scale (zonal wavenumbers 1–3) and have periods which are of the order of a week or more. These low-frequency, low wavenumber waves

¹ Contribution No. 651, Department of Atmospheric Sciences, University of Washington.

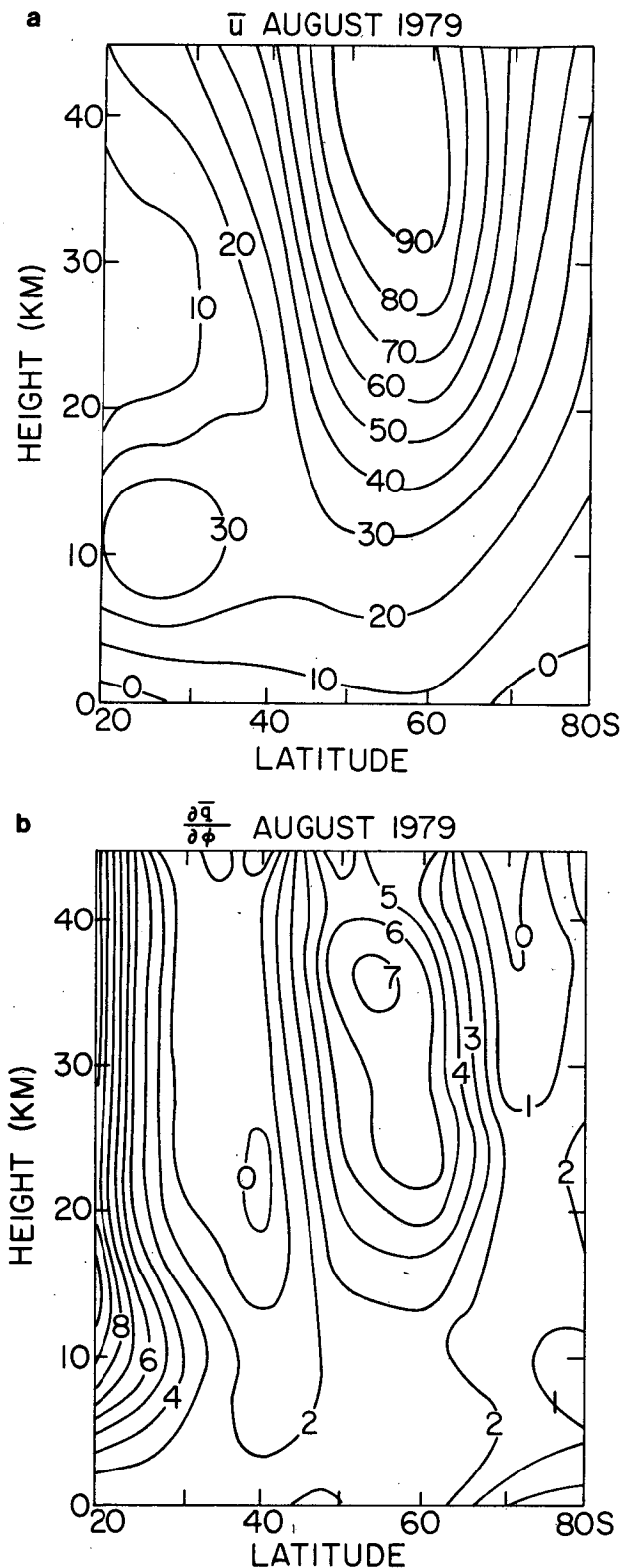


FIG. 1. Height versus latitude contour plots of (a) zonal-mean wind (m s^{-1}) and (b) the smoothed gradient of potential vorticity (divided by $\Omega = 7.292 \times 10^{-5} \text{ s}^{-1}$) for the month of August 1979 in the Southern Hemisphere.

are similar in space and time behavior to the dominant observed waves in the stratosphere, particularly in the Southern Hemisphere where negative mean potential vorticity gradients are most frequently observed. These *in situ* instabilities may interact strongly with the planetary waves propagating upward from the troposphere.

2. Source of the instability

The zonal mean wind in the Southern Hemisphere during August 1979 and a smoothed representation of the meridional gradient of quasi-geostrophic potential vorticity during the same period are shown in Fig. 1. Of note are the regions of small or negative potential vorticity gradient at about 40°S and 70°S on the flanks of the polar night jet stream which is centered at about 55°S. Similar features are present during June and July. One can argue that these regions of large positive zonal wind curvature and hence small potential vorticity gradient are continually forced by radiative processes. Radiative equilibrium-temperature distributions for winter conditions near the stratopause show very sharp gradients near the boundary of winter polar darkness where the insolation goes to zero, and much weaker gradients poleward and equatorward of this latitude (e.g., Leovy, 1964, Fig. 7). This distribution of temperature implies a very sharp jet in high latitude with regions of small or negative potential vorticity gradient on its flanks. Dynamical processes other than instability could alter this wind profile to remove the regions of negative vorticity gradient before instability sets in, but Fig. 1 suggests that, even in monthly mean cross sections, some regions of negative potential vorticity gradient remain.

Kuo (1949) has shown that in a barotropic, non-divergent fluid on a sphere a zero in the gradient of absolute vorticity is a necessary condition for the instability of a zonal wind profile. In this paper it will be demonstrated that barotropic instability of zonal mean wind profiles like those found near the stratopause region gives rise to waves with the observed features of the 4-day wave described by VS. Moreover, it will be suggested that there may also be an eastward moving wavenumber 2 with period of 1–2 days near the polar winter stratopause whose period is too short to be resolved by their analysis. These waves are associated with the region of negative vorticity gradient near the pole and are confined to the polar side of the jet axis. In addition there are unstable modes associated with the regions of negative mean potential vorticity gradient near 40°S. These modes have significant growth for the lowest zonal wavenumbers and have broad meridional scales with amplitude maxima near the latitude of the jet axis. The periods for these mid-latitude unstable modes are in the range from 1 to 3 weeks.

3. The barotropic nondivergent model

a. Formulation

The linearized barotropic nondivergent vorticity equation may be written

$$\frac{\partial \zeta'}{\partial t} + \bar{\omega} \frac{\partial \zeta'}{\partial \lambda} + \frac{v'}{a} \frac{\partial \bar{Z}}{\partial \phi} = 0. \tag{1}$$

Choosing a stream function of the form

$$\psi = \hat{\psi}(\phi) \exp[i(m\lambda - \sigma t)], \tag{2}$$

(1) becomes

$$(m\bar{\omega} - \sigma) \left[\frac{1}{\cos\phi} \frac{\partial}{\partial \phi} \left(\cos\phi \frac{\partial \hat{\psi}}{\partial \phi} \right) - \frac{m^2 \hat{\psi}}{\cos^2\phi} \right] + \frac{m}{\cos\phi} \frac{\partial \bar{Z}}{\partial \phi} \hat{\psi} = 0. \tag{3}$$

Here

- λ latitude,
 - $\bar{\omega}$ $\bar{u}(a \cos\phi)^{-1}$ is the relative angular velocity of the zonal mean flow,
 - a the radius of the earth
 - m the zonal wavenumber
 - σ the frequency.
- $\frac{\partial \bar{Z}}{\partial \phi} = 2(\Omega + \bar{\omega}) \cos\phi + 3 \sin\phi \frac{\partial \bar{\omega}}{\partial \phi} - \cos\phi \frac{\partial^2 \bar{\omega}}{\partial \phi^2}$ is

the absolute vorticity gradient.

We solve for the unstable modes by finite differencing (3) and then solving the resulting matrix eigenvalue problem for the complex frequencies and their associated eigenvectors. All results presented here were obtained using a 1.5 degree grid spacing which was adequate to determine the eigenvalues and structure of the most unstable modes.

The eigenvalue problem (3) produces values of $\sigma = \sigma_r + i\sigma_i$ with real and imaginary parts σ_r and σ_i respectively. To facilitate comparisons with observation we will present the eigenvalues in terms of the e -folding time

$$\tau_i = (\sigma_i)^{-1} \tag{4}$$

and the real period

$$\tau_r = 2\pi(\sigma_r)^{-1}, \tag{5}$$

which will be presented in units of solar days (86400 s). For the wind profiles studied here, the phase speeds of all the unstable modes are eastward, which corresponds to positive frequency and period.

b. Growth rates and phase speeds

In order to simplify the study of barotropic instabilities near the polar stratopause we will choose a meridional variation of the wind of the following simple analytic form:

$$\bar{\omega} = \bar{u}(a \cos\phi)^{-1} = Ua^{-1} \operatorname{sech}[2.0(\phi - \phi_0)B^{-1}]. \tag{6}$$

Here Ua^{-1} is the maximum relative angular velocity which occurs at the latitude $\phi = \phi_0$ and B measures the width of the jet.

Zonal wind profiles which are similar to those in Fig. 1 can be obtained by setting $U = 180 \text{ m s}^{-1}$, $\phi_0 = 60^\circ$ and varying B over the range 10 to 35. The zonal winds and vorticity gradients corresponding to these choices are shown in Fig. 2. For small values of B the jet is very sharp and there are regions of negative absolute vorticity gradient both on the poleward and equatorward sides of the jet. For larger values of $B \geq 20$ there is a region of negative absolute vorticity gradient only on the poleward side of the jet where the planetary vorticity gradient is small. Regions of negative vorticity gradient are required for instability of the zonal mean state, and the growth rate, period, and structure of the growing waves depend critically on the position and intensity of these regions.

Table 1 displays the general behavior of the most unstable modes for the wind profiles shown in Fig. 2. There are two classes of unstable modes present when B is small enough that there are two regions of negative absolute vorticity gradient. One class is associated with the region of negative vorticity gradient on the equatorward flank of the jet. The e -folding times and periods for these modes are enclosed in parentheses in Table 1. They generally have higher growth rates for higher zonal wavenumbers than modes associated with the region of negative vorticity gradient poleward of the jet center, and, for the same zonal wavenumber, have longer periods. The structural features associated with these differences will be discussed in the next section.

For broad jets ($B \geq 15$) and for modes associated with the regions of negative absolute vorticity on the poleward flank of the jet (for convenience let us call them polar modes hereafter), significant growth rates ($\tau_i \leq 7$ days) occur only for zonal wavenumbers 1 and 2. The growth rates decrease as the jets become more broad and the regions of negative vorticity gradient become smaller and weaker. The periods, however, are relatively insensitive to the breadth of the jet.

Fig. 3 shows wind profiles and vorticity gradients for $B = 20$, $\phi_0 = 60$ and U varying over the range of 90 to 240 m s^{-1} . As shown in Table 2, increasing the intensity of the jet increases the growth rate of the waves and decreases their period. Values of U which produce wind profiles comparable to those observed, produce periods for the most unstable mode of zonal wavenumber 1 which are very close to the spectral peak observed by VS at about 3.5 days. Note, however, that for many reasonable wind profiles wavenumber 2 has growth rates comparable to wavenumber 1. Venne and Stanford (1982) do not report a

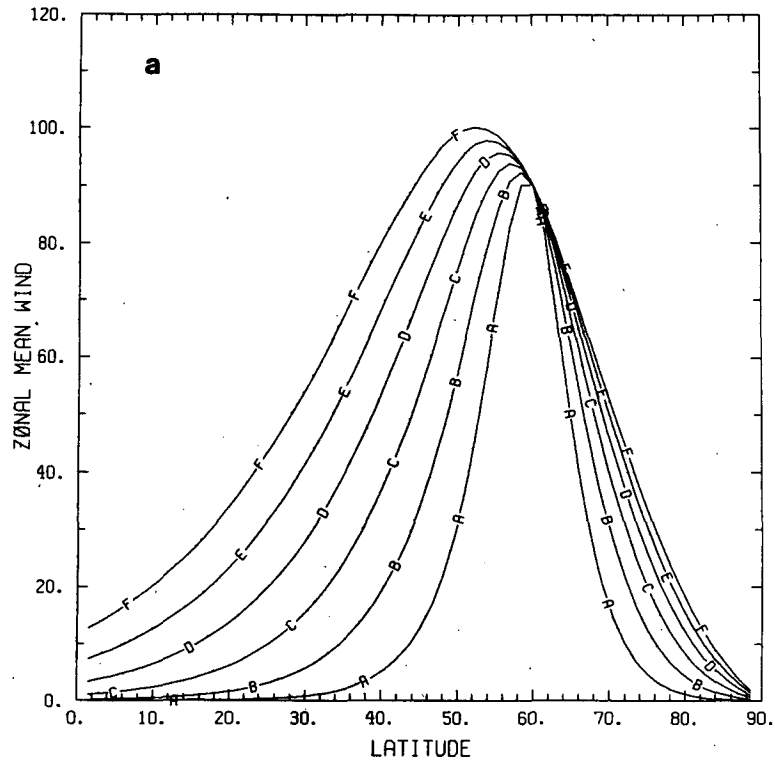
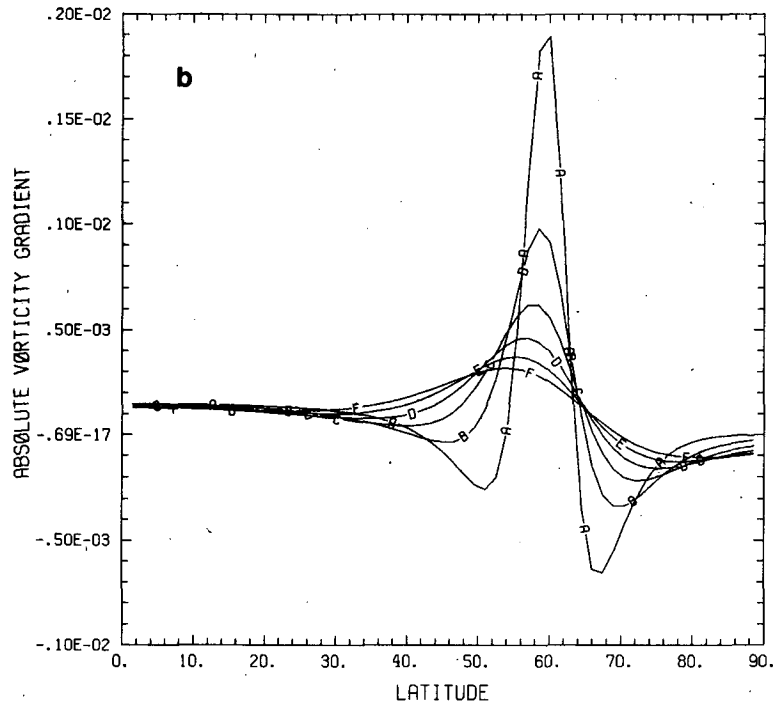
ZONAL WIND, $U_2 = 180.$, $Y_2 = 60.$ VORT. GRAD, $U_2 = 180.$, $Y_2 = 60.$ 

FIG. 2. Line graphs of (a) zonal wind speed and (b) absolute vorticity gradient $\partial\bar{z}/\partial\phi$ for analytic wind profiles of the form $\bar{\omega} = (U/a) \operatorname{sech}(2(\phi - \phi_0)/B)$ with $U = 180 \text{ m s}^{-1}$, $\phi_0 = 60^\circ$, and B varying over the values 10, 15, 20, 25, 30, and 35, indicated by the curves marked A through F, respectively.

TABLE 1. The e -folding time τ_i and real period τ_r in days for the most unstable modes produced by the nondivergent barotropic model for the jet profile given by (6) with $U = 180$, $\phi_0 = 60$, and various values of B and zonal wavenumber m . Values enclosed by parentheses are for modes associated with the presence of a region of negative absolute vorticity gradient on the equatorward side of the jet.

B	Zonal wavenumber (m)													
	1		2		3		4		5		6		7	
	τ_i	τ_r	τ_i	τ_r	τ_i	τ_r	τ_i	τ_r	τ_i	τ_r	τ_i	τ_r	τ_i	τ_r
10	4.5	2.9	2.5	1.6	2.9	1.1	—	—	6.6	0.72	4.0	0.60	3.1	0.50
	—	—	(6.3)	(16)	(1.2)	(3.2)	(1.1)	(1.7)	(1.4)	(1.1)	—	—	—	—
15	4.9	3.0	4.1	1.6	—	—	12	0.85	7.3	0.68	7.0	0.56	—	—
	—	—	—	—	(5.0)	(2.7)	—	—	—	—	—	—	—	—
20	5.7	3.0	6.9	1.6	—	—	18	0.83	13	0.66	—	—	—	—
25	6.9	3.0	11	1.6	—	—	30	0.81	43	0.65	—	—	—	—
30	8.4	3.0	17	1.6	—	—	64	0.80	—	—	—	—	—	—
35	22.0	2.9	—	—	—	—	—	—	—	—	—	—	—	—

wavenumber 2 in the polar stratopause region, but the Nyquist period for their spectral analysis was 2.0 days so that they could not resolve the expected period for this wave, which would be less than 2 days. The presence of a wavenumber 2 mode with a period of 1.5–2 days is suggested in their analysis by the large amount of noise indicated for wavenumber 2 at periods near 2 days in the Southern Hemisphere (their Fig. 2). An analysis which fully utilized the twice daily data from satellites would push the Nyquist period to 1.0 days. Such an analysis would allow one to determine whether rapidly eastward moving polar modes were present for wavenumber 2 and possibly 3, and should be undertaken.

c. Structure of the unstable modes

The structures of selected unstable modes for the barotropic nondivergent model (3) are shown in Figs. 4–6. In presenting the structure we plot the amplitude of the streamfunction normalized so that its maximum value is unity and the phase of the streamfunction divided by π so that the values of the phase range from -1 to $+1$. Also plotted are the zonal mean poleward momentum flux $u'v'$, and the convergence of the poleward momentum flux, $-\partial u'v'/\partial y$, which for the model (1) is also the poleward vorticity flux $v'\zeta'$ and the divergence of the Eliassen–Palm flux $\nabla \cdot \mathbf{F}$ (Edmon *et al.*, 1980). The significance of the latter quantity can be illustrated by considering the enstrophy budget for the nondivergent barotropic model, which is easily derived from (1).

$$\begin{aligned} \frac{\partial}{\partial t} \frac{1}{2} \overline{\zeta'^2} &= -\overline{v'\zeta'} \frac{1}{a} \frac{\partial Z}{\partial \phi} \\ &= \frac{1}{a^2 \cos^2 \phi} \frac{\partial}{\partial \phi} (\overline{u'v'} \cos^2 \phi) \frac{\partial Z}{\partial \phi} \\ &= \frac{-\nabla \cdot \mathbf{F}}{a \cos \phi} \frac{\partial Z}{\partial \phi}, \end{aligned} \tag{7}$$

where $\mathbf{F} = (F_\phi, 0)$ and $F_\phi = -a \cos \phi \overline{u'v'}$.

It is clear from (7) that in order for a wave to grow in amplitude with time, its structure must be such as to give an Eliassen–Palm flux divergence which is of opposite sign to the absolute vorticity gradient, at least in a globally integrated sense. For the unstable modes found here, the Eliassen–Palm flux divergence and absolute vorticity gradient are of opposite sign at every point. The relation described by (7) can be generalized to quasi-geostrophic disturbances by replacing ζ' with the quasi-geostrophic potential vorticity perturbation and \bar{Z} with the zonal mean quasi-geostrophic potential vorticity.

In describing the structure of unstable modes of the nondivergent barotropic model we will present streamfunction amplitude, phase, poleward momentum flux, and Eliassen–Palm flux divergence divided by cosine of latitude. We divide the E–P flux divergence by cosine of latitude because of its appearance in this form in (7) and in the zonal mean wind equation for this model, which is

$$\frac{\partial \bar{u}}{\partial t} = -\frac{1}{a \cos^2 \phi} \frac{\partial}{\partial \phi} (\overline{u'v'} \cos^2 \phi) = \frac{\nabla \cdot \mathbf{F}}{a \cos \phi} \tag{8}$$

The structures of the most unstable modes for zonal wavenumbers 1, 2, and 3 growing on a wind profile defined by (6) with $U = 180$, $\phi_0 = 60$, and $B = 15$ are shown in Figs. 4, 5, and 6, respectively. Wavenumbers 1 and 2 have similar structure with amplitude maxima at high latitude near 70° . The phase shifts rapidly westward on the equatorward side of the amplitude maximum so that a large poleward momentum flux is produced in that region. The E–P flux divergence is everywhere of opposite sign to the zonal mean absolute vorticity gradient. For the wind profile used in the cases shown in Figs. 4–6 the absolute vorticity gradient changes sign at 65 , 48 , and 41 degrees of latitude. Where it is of significant magnitude, it can be seen that the E–P flux divergence also changes sign at each of these latitudes, so that its sign remains opposite to that of the absolute vorticity gradient as is required for growing modes.

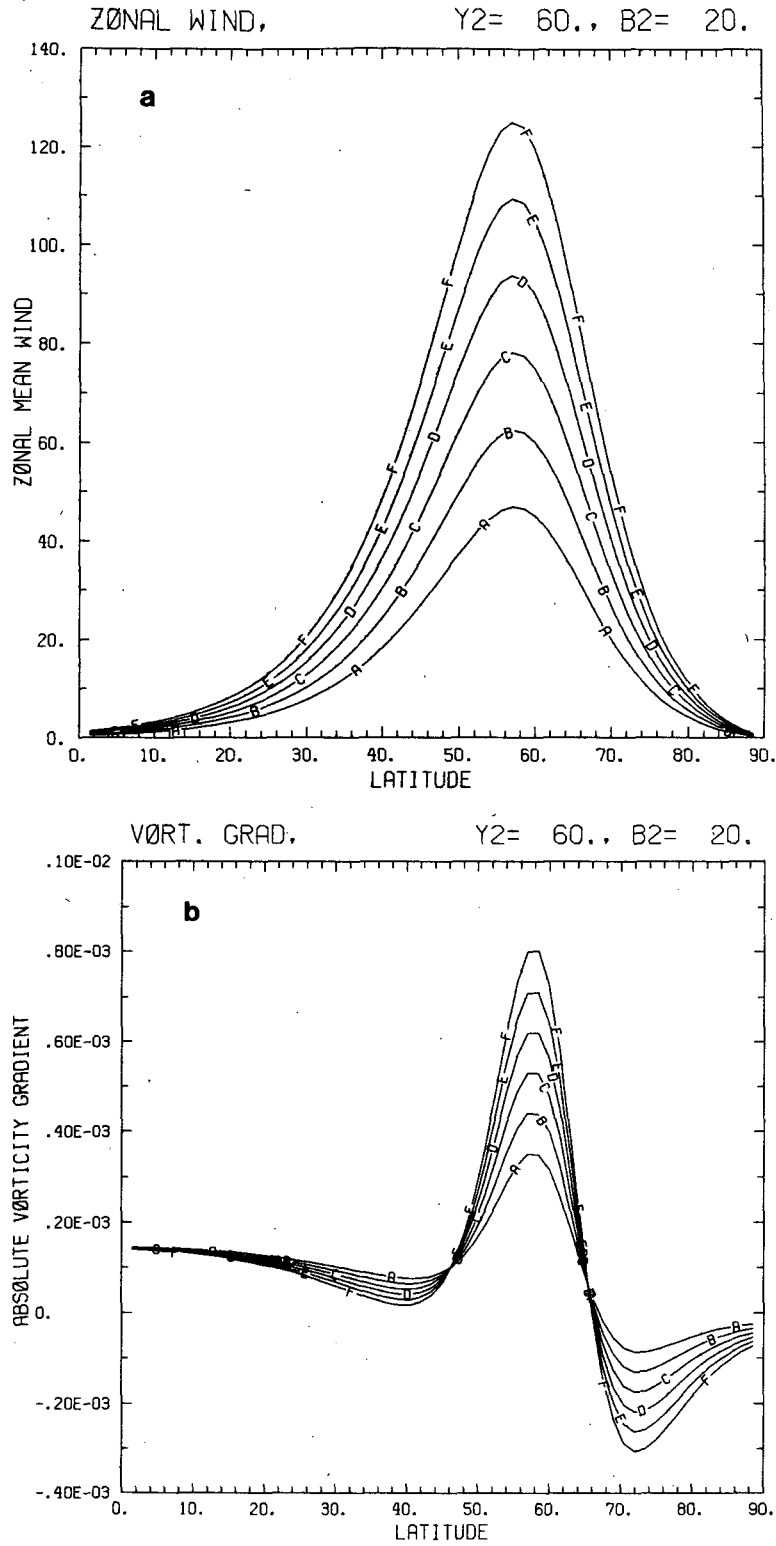


FIG. 3. As in Fig. 2 but for $B = 20$, $\phi_0 = 60^\circ$, and U varying over the values 90, 120, 150, 180, 210, and 240, indicated by A through F, respectively.

Wavenumber 3 (Fig. 6) is different from wavenumbers 1 and 2 (Figs. 4 and 5) in that its momentum flux is predominantly equatorward and its E-P flux

divergence is large in the vicinity of the mid-latitude region of negative absolute vorticity gradient equatorward of the jet. This mode is associated with the

TABLE 2. Same as Table 1 except for various values of U with $B = 20$, $\phi_0 = 60$, and only zonal wavenumbers 1 and 2.

U	Zonal wavenumber (m)			
	1		2	
	τ_i	τ_r	τ_i	τ_r
90	12.3	6.6	19.2	3.5
120	8.5	4.7	16.6	2.6
150	6.8	3.7	10.0	1.9
180	5.7	3.0	6.9	1.6
210	5.0	2.5	5.5	1.4
240	4.4	2.2	4.5	1.2

presence of the mid-latitude region of negative absolute vorticity gradient and does not appear when the region is absent, as in the cases with $B \gtrsim 20$.

It should be noted that all the modes have critical lines ($m\bar{\omega} - \sigma = 0$) near a latitude where the absolute vorticity gradient is zero. This latitude also corresponds to that with the momentum flux of largest magnitude. Wave over-reflection ideas can be used to gain an intuitive notion of why this structure is required (Lindzen and Tung, 1978). Tung (1981) has also presented an argument which suggests that the

potential vorticity gradient and the Doppler-shifted frequency, $m\bar{\omega} - \sigma$, should be of the same sign for unstable disturbances in a closed domain. Since the wavenumber 3 mode has a critical line in a region with a smaller relative angular velocity than the regions where the wavenumber 1 and 2 modes must have critical lines, its period is comparatively longer. This effect may enhance the importance of the equatorward region of negative vorticity gradient in the stratosphere, since for planetary-scale waves it places the frequency of the unstable normal modes close to the frequency of the forced waves in the stratosphere.

d. Mid-latitude modes

In order to isolate the modes associated with regions of negative mean absolute vorticity gradient on the equatorward side of the polar night jet we study a shear wind profile of the following form:

$$\bar{\omega} = \frac{1}{2} U a^{-1} \{1 + \tanh[(\phi - \phi_0)B^{-1}]\}. \quad (9)$$

This provides a region of negative vorticity gradient only on the equatorward side of the jet axis. Wind profiles and vorticity gradients for $U = 180$ and $\phi_0 = 45$ and several values of B are shown in Fig. 7.

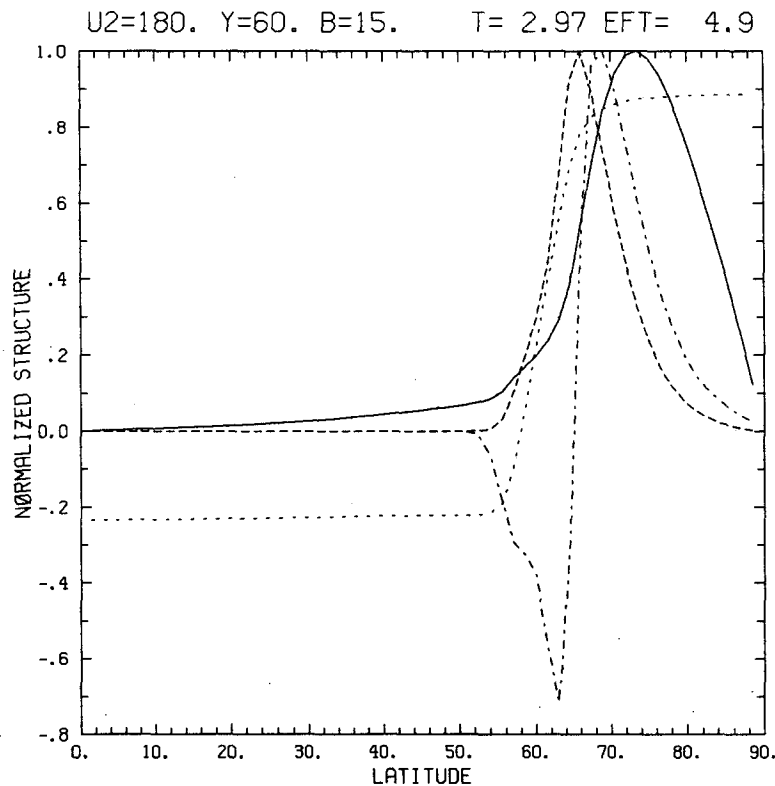


FIG. 4. Structure of the most unstable mode of wavenumber 1 for a zonal wind profile defined by (6) with $U = 180$, $\phi_0 = 60$, and $B = 15$. Normalized amplitude (solid line), phase (dotted line, positive to the east), poleward momentum flux (dashed line), and Eliassen-Palm flux divergence divided by cosine of latitude (dash-dot line) are shown as functions of latitude.

U2=180. Y=60. B=15. T= 1.64 EFT= 4.1

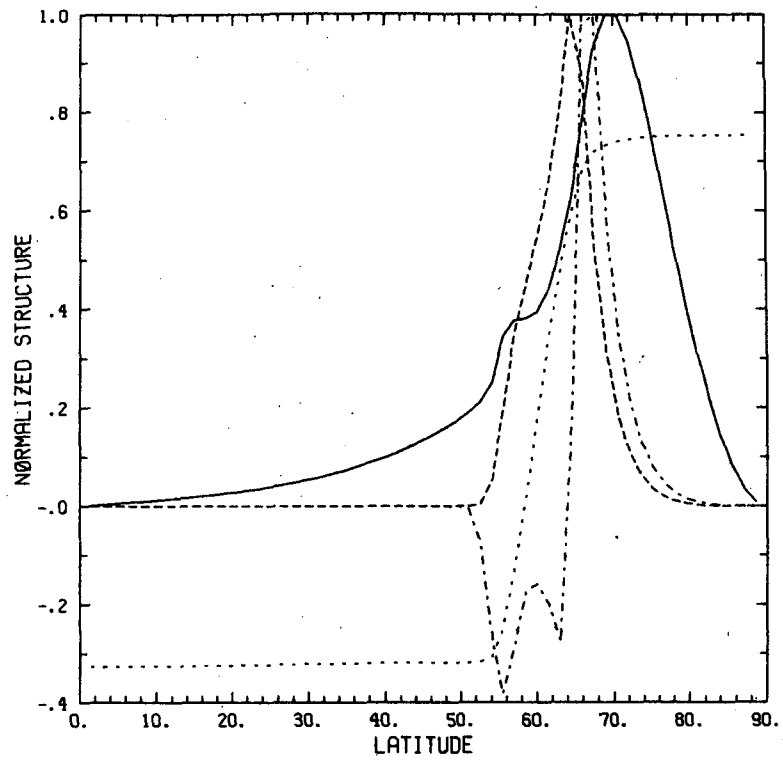


FIG. 5. As in Fig. 4 except for wavenumber 2.

U2=180. Y=60. B=15. T= 2.75 EFT= 5.0

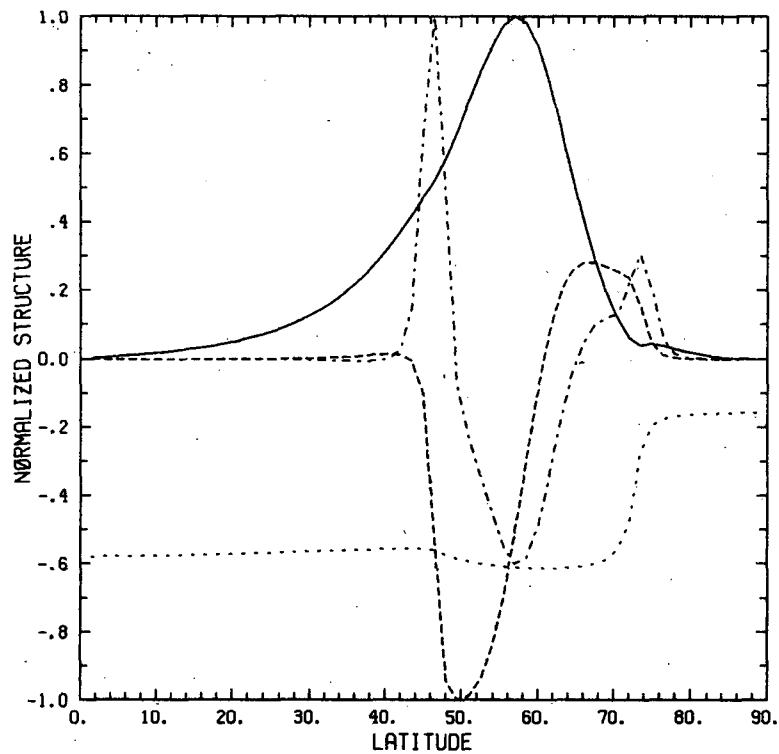


FIG. 6. As in Fig. 4 except for wavenumber 3.

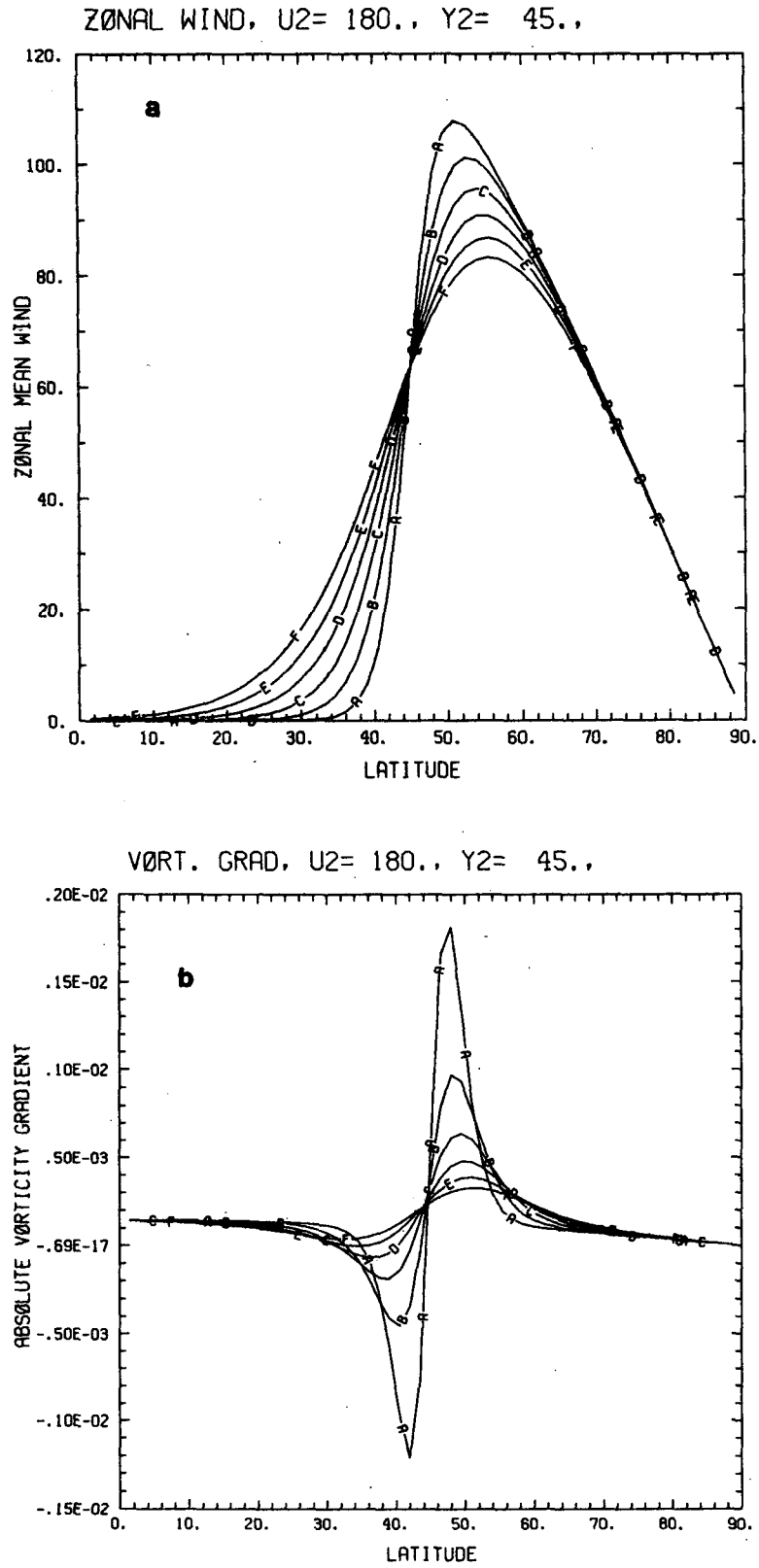


FIG. 7. Line graphs of (a) zonal wind speed and (b) absolute vorticity gradient for shear zone wind profiles of the form (9) with $U = 180$, $\phi_0 = 60$, and B varying over the values 4, 6, 8, 10, 12, and 14, indicated by the curves marked A through F, respectively.

TABLE 3. Same as Table 1 except for the unstable modes produced for the shear zone wind profile given by (9) with $U = 180$ and $\phi_0 = 45$.

B	Zonal wavenumber (m)															
	1		2		3		4		5		6		7		8	
	τ_i	τ_r	τ_i	τ_r	τ_i	τ_r	τ_i	τ_r	τ_i	τ_r	τ_i	τ_r	τ_i	τ_r	τ_i	τ_r
4	—	—	1.2	12	0.57	3.3	0.47	1.9	0.46	1.9	0.49	1.1	0.56	0.90	0.72	0.78
6	—	—	1.8	14	0.82	3.5	0.79	2.0	1.0	1.4	2.6	1.1	—	—	—	—
8	—	—	3.6	17	1.3	3.7	1.8	2.1	20	1.5	—	—	—	—	—	—
10	—	—	4.8	21	3.1	4.0	—	—	—	—	—	—	—	—	—	—
12	—	—	—	—	—	—	—	—	—	—	—	—	—	—	—	—

Table 3 shows the e -folding times and real periods for the unstable modes growing on the hyperbolic tangent profile (9) with $U = 180$, $\phi_0 = 45$, and various values of B . For very sharp shear zones and accompanying regions of substantially negative gradient of absolute vorticity (e.g., $B = 4$) the most rapid growth rates occur at synoptic scales (e.g., $m = 5$) and the modes have very short periods. For broader shear zones (e.g., $B = 10$) the most rapid growth occurs for planetary scales (e.g., $m = 2$ or 3) and the periods are much longer. For zonal wavenumber 2 the period of the unstable mode is 2–3 weeks, which is near the observed dominant period of eastward moving wavenumber 2 in the Southern Hemisphere (e.g., Hart-

mann, 1976; Leovy and Webster, 1976). Even for very sharp shear zones the e -folding times of zonal wavenumber 2 are only slightly more than double the e -folding time of the most unstable wavenumber. Since the amplitudes of zonal wavenumbers 2 and 3 in the stratosphere are always larger than higher wavenumbers due to continual forcing from the troposphere, one might expect the planetary-scale barotropically unstable modes to be more important than synoptic scales, because, though their growth rates are slower, their initial amplitudes are much larger on average.

Fig. 8 shows the structure of the unstable mode of wavenumber 2 for a wind profile with $U = 180$, ϕ_0

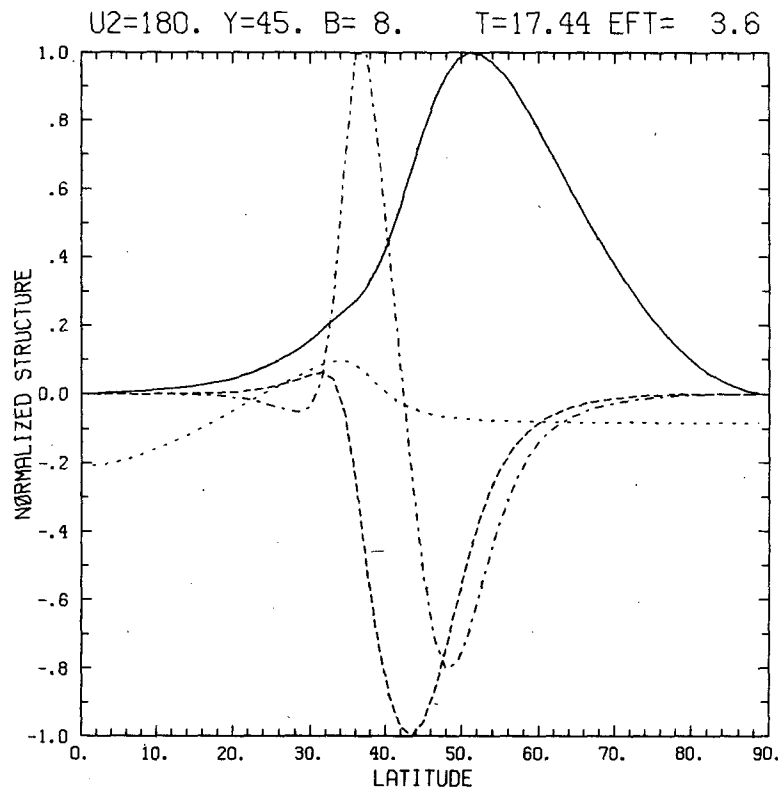


FIG. 8. Structure of the unstable mode of wavenumber 2 for the shear zone wind profile given by (9) with $U = 180$, $\phi_0 = 45$, and $B = 8$. See caption to Fig. 4 for further details.

$= 45$, and $B = 8$. The streamfunction has its maximum amplitude slightly equatorward of the jet core. The phase of the wave is relatively constant everywhere except in the region of negative vorticity gradient where there is a westward shift of about $\pi/10$ radians in 10 degrees of latitude. This phase shift produces an equatorward momentum transport centered at about 44 degrees of latitude. The unstable modes for higher zonal wavenumbers have similar structures, as does the example shown in Fig. 5 for wavenumber 3 growing on a hyperbolic secant wind profile. There are no unstable modes for wavenumber 1 and the wind profiles given in Fig. 7. This is perhaps because the nondivergent barotropic modes for wavenumber 1 retrogress too rapidly to allow a critical line to form at the required latitude, so that unstable modes do not exist. The β -plane results of Dickinson and Clare (1973) show a long wave cutoff to instability, which occurs at shorter wavelengths for larger values of β . We shall see in the next section that a divergent baroclinic model does have a growing mode for wavenumber 1.

The effect of varying the latitude of the shear zone on the wind profiles is shown in Fig. 9. The e -folding times and periods for these cases are shown in Table 4. A shear zone in low latitudes favors higher wavenumbers, while one in middle or high latitudes favors low wavenumbers. A shear zone at 45° produces a region of negative absolute vorticity gradient at about the observed latitude and gives rise to significant growth rates for wavenumbers 2, 3, and 4.

e. Higher order modes

The barotropic instability of hyperbolic tangent shear-zone wind profiles like (9) has been studied on a β -plane by Garcia (1956), Michalke (1964), Kuo (1973), and others. Following a suggestion posited by Howard and Drazin (1964) that there might be more than one unstable mode on a β -plane, Dickinson and Clare (1973) performed a detailed study of this profile on a β -plane and found a second unstable mode with a slower growth rate but better meridional propagation than the most unstable mode. We found only one unstable mode for the shear zone profile for each zonal wavenumber. While Eq. (1) can be made to appear formally equivalent to its form on a β -plane through a Mercator projection (e.g., Kuo, 1949), the two problems are not equivalent because of the variation of β in the fully spherical case and the application of no-flux boundary conditions at the poles. The no-flux boundary conditions applied on the sphere exclude the propagating mode of Dickinson and Clare (1973), as noted by Tung (1981). The most unstable mode seems to have the broadest meridional scale which will fit within the region of propagation on the sphere. [An argument for why this should be so in the case of forced waves has been given by Boyd (1982).] In the propagating regions the planetary vor-

ticity gradient and the Doppler-shifted phase speed must be of the same sign. The region of propagation for the polar modes extends from the strong zonal winds on the poleward side of the jet in high latitudes to the pole, where a no-flux boundary condition must be applied. The mid-latitude modes propagate in the region from the equatorward edge of the mid-latitude region of the negative potential vorticity gradient to the pole (or to a possible region of reversed vorticity gradient in high latitudes). For unstable modes of either type there is generally a critical line coincident with a vorticity gradient reversal within the region of propagation.

For the jet profile (6), higher modes were frequently found in association with the polar region of negative vorticity gradient. These modes had much slower growth rates than the most unstable mode, but similar periods. Their structure was characterized by a higher degree of meridional structure than the most unstable mode, which was brought about by amplitude nodes and phase reversals at one or more critical lines. Because their e -folding times are long compared to the dissipation time scale in the stratosphere and their structure is conducive to rapid dissipation by lateral diffusion, these modes are not thought to be physically important and hence are not discussed further in this paper.

4. Effects of Divergence and Baroclinicity

a. The quasi-geostrophic model

In order to consider the effects of divergence and baroclinicity and to provide more detail on the expected structure of barotropic instabilities, we present here a few results obtained using a quasi-geostrophic model. The model and its use in obtaining growth rates and structure of unstable modes are described in Hartmann (1979). In the calculations described here, a finite difference grid of 5 km in height by 2.0 or 2.5 degrees in latitude was used. Boundary conditions of vanishing geopotential height at the polar, equatorial, and upper (90 km) boundaries and vanishing vertical velocity at the ground were applied. A time step of two hours was used. A 260 K isothermal basic temperature profile was assumed, and uniform Newtonian cooling with a time scale of 20 days was applied.

b. Polar modes

Fig. 10 shows the geopotential height amplitude and phase for a zonal wind speed which is independent of height, but which has a meridional variation as in (6) with $U = 180$, $\phi_0 = 60$, and $B = 20$. The e -folding time obtained with the quasi-geostrophic model was 7.2 days and the period was 3.1 days. These values compare well with the results of the nondivergent barotropic eigenvalue problem which gave 5.7 and 3.0 days, respectively. The geopotential

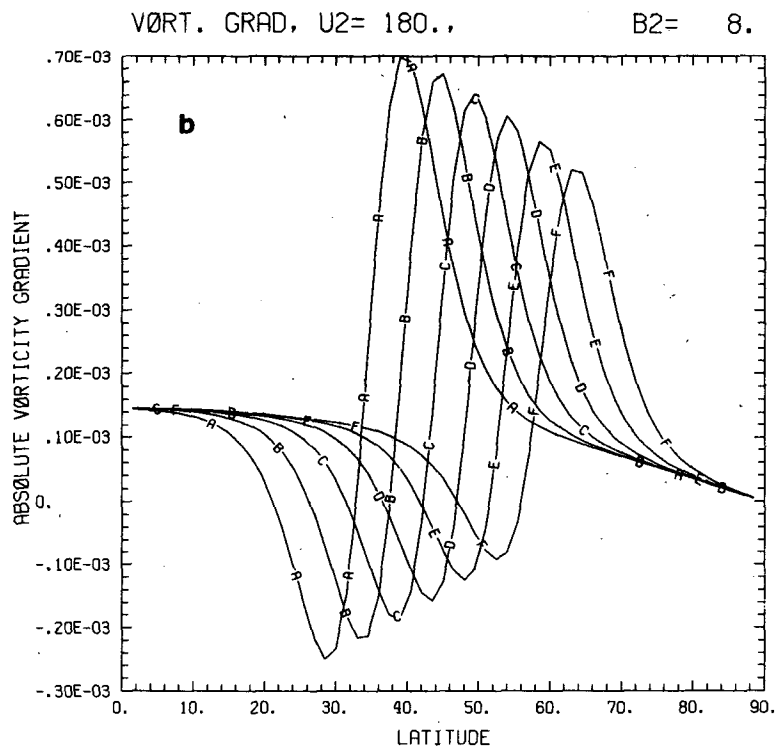
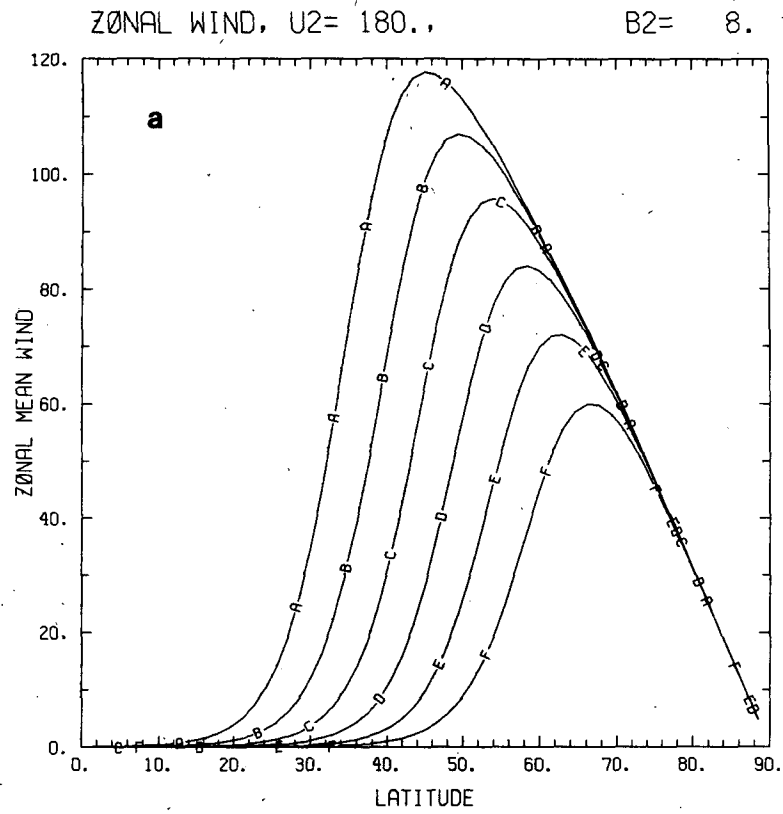


FIG. 9. Line graphs of (a) zonal wind speed (m s^{-1}) and (b) absolute vorticity gradient (s^{-1}) for shear zone wind profiles given by (9) with $U = 180$, $B = 8$, and ϕ_0 varying over the range 35, 40, 45, 50, 55, and 60, indicated by the curves marked A through F, respectively.

TABLE 4. Same as Table 3 except for $U = 180, B = 8$, and various values of ϕ_0 .

ϕ_0	Wavenumber													
	1		2		3		4		5		6		7	
	τ_i	τ_r	τ_i	τ_r	τ_i	τ_r	τ_i	τ_r	τ_i	τ_r	τ_i	τ_r	τ_i	τ_r
35	—	—	55	37	1.1	3.9	1.1	2.1	1.9	1.5	—	—	—	—
40	—	—	5.6	23	1.2	3.8	1.4	2.1	4.7	1.5	—	—	—	—
45	—	—	3.6	17	1.3	3.7	1.8	2.1	20	1.5	—	—	—	—
50	—	—	3.0	14	1.6	3.7	2.9	2.1	—	—	—	—	—	—
55	—	—	2.9	12	2.1	3.6	8.0	2.2	—	—	—	—	—	—
60	—	—	3.1	10	3.7	3.6	—	—	—	—	—	—	—	—

height has been normalized to a maximum amplitude of 100 meters and the phase is given in degrees measured positive to the east. The maximum amplitude occurs at about 75° latitude, and would increase monotonically to the top of the model except for the boundary condition of zero geopotential height which has been applied at 90 km. The energy density actually decreases slightly with altitude away from a maximum at the ground in this case. The phase variation is very similar to that obtained in Figs. 4 and 5, with rapid westward shift with decreasing latitude equatorward of the amplitude maximum.

To investigate the role of vertical shear we introduce a zonal mean wind cross section of the following form:

$$\bar{\omega} = Ua^{-1} \operatorname{sech}[2(\phi - \phi_0)B^{-1}] \times \operatorname{sech}[2(Z - Z_0)A^{-1}]. \quad (10)$$

Fig. 11 shows the zonal mean wind and quasi-geostrophic potential vorticity gradient for a cross section given by (10) with $\phi_0 = 60^\circ, U = 180, B = 20, Z_0 = 50$ km, and $A = 75$ km. In order to suppress baroclinically unstable modes, the wind profile (10) was modified to be independent of height in the top three and bottom three layers.

The structure of the most unstable mode of wavenumber 1 obtained for this wind cross-section is given in Fig. 12. The amplitude maximum now appears about 1 scale height above the level of maximum wind. The heat transport associated with this mode is weak and poleward above the jet axis and equatorward below. This implies a vertical flux of energy away from the jet axis and also stabilizing baroclinic energy conversions. More important, however, is the momentum transport, which is strongly poleward, implying equatorward energy flux and barotropic conversions from the zonal mean to the eddy component. This is confirmed by the E-P flux divergence (again divided by cosine of latitude, and the quasi-geostrophic form of Edmon *et al.* (1980) has been used) which indicates that a 100 m amplitude wave produces a rather significant zonal mean acceleration of nearly $3 \text{ m s}^{-1} \text{ day}^{-1}$. The temperature perturbation associated with a normal mode of 100 m amplitude has a rather small ($<1.5 \text{ K}$) maximum at 45 km, 75°

latitude (not shown). The e -folding time and period associated with the mode shown in Fig. 12 are 9.3 and 3.2 days, respectively. Higher wavenumbers exhibit no instability for these conditions. The wind profile in Fig. 11 is thus near neutral stability, which is perhaps a realistic average condition for the atmosphere at the stratopause. For this case the period of 3.2 days is close to the central period of 3.5 days found by VS. Note that the e -folding time increases from 7.2 to 9.3 days when the parameter A is decreased from infinity to 75 km. This is consistent with the results of Pfister (1979) who found that the vertical curvature of the wind profile reduces growth rates. It seems natural that this should be the case, since the magnitudes of the negative vorticity gradients are reduced away from the jet core. The baro-

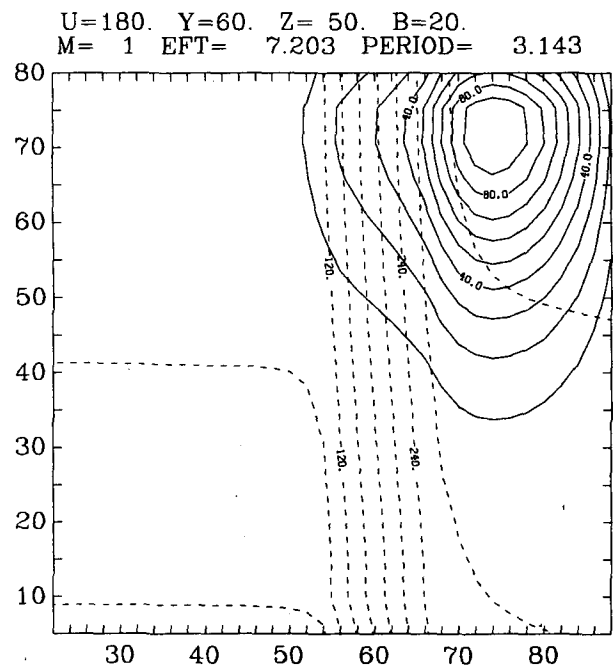


FIG. 10. Height (ordinate, in km) versus latitude (abscissa, degrees) contour plots of normalized geopotential height amplitude (solid contours, interval 10 m) and phase (dashed contours, interval 30°) for the most unstable mode of zonal wavenumber 1 growing on a zonal wind with a horizontal distribution given by (6) with $U = 180, \phi_0 = 60$, and $B = 20$. Compare to Fig. 4.

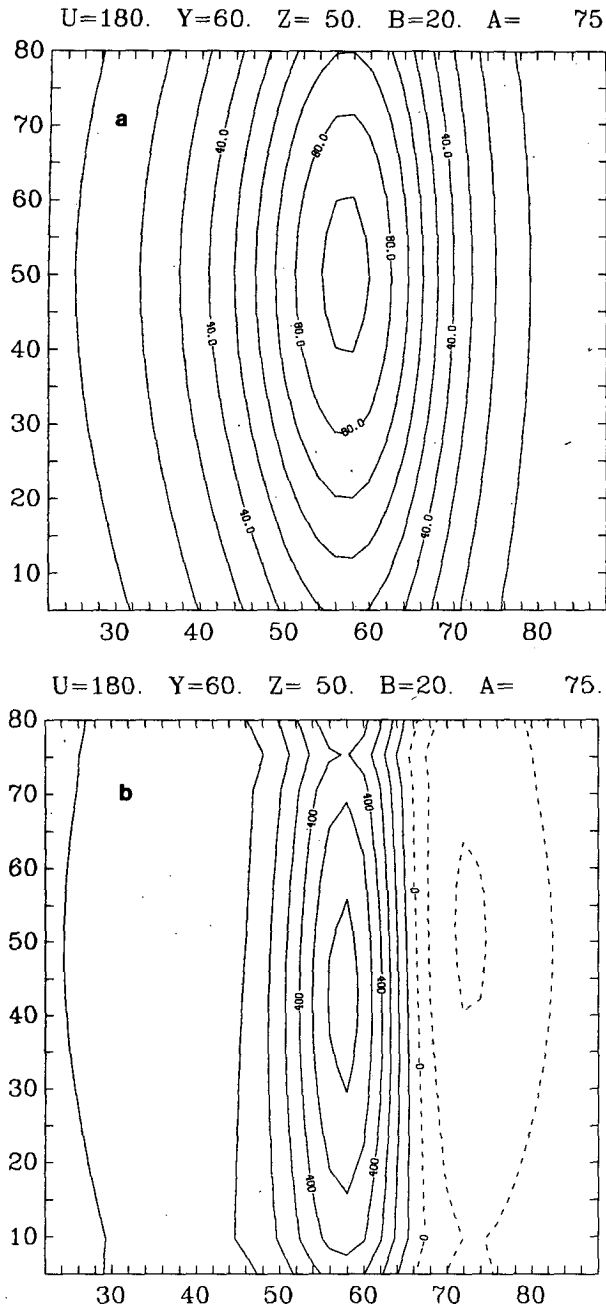


FIG. 11. Height versus latitude contour plots of (a) zonal-mean wind (contour interval 10 m s^{-1}) and (b) quasi-geostrophic potential vorticity gradient (contour interval $1 \times 10^{-3} \text{ s}^{-1}$) for the jet profile given by (10) with $U = 180$, $\phi_0 = 60$, $B = 20$, $Z_0 = 50$, and $A = 75$.

clinic energy conversions associated with the flux of energy away from the level of the jet maximum tend to offset the barotropic energy conversions associated with the instability.

c. Mid-latitude modes

To investigate the three-dimensional structure of unstable modes associated with a region of negative

potential vorticity gradient on the equatorward side of the polar night jet, we employ a zonal wind profile of the following form:

$$\bar{\omega} = \frac{1}{2} U a^{-1} \{1 + \tanh[(\phi - \phi_0) B^{-1}] \times \text{sech}[2(Z - Z_0) A^{-1}]\}. \quad (11)$$

Fig. 13 shows the wind and quasi-geostrophic potential vorticity gradient for the wind profile (11) with $U = 180$, $\phi_0 = 45$, $B = 8$, $Z = 50 \text{ km}$, and $A = 75$. The structure for the unstable mode of wavenumber 2 growing on the basic state shown in Fig. 13 is given in Fig. 14. As in the barotropic case there is a broad amplitude maximum and only modest phase changes with latitude. There is a region of equatorward momentum flux which gives rise to a dipole pattern in the E-P flux divergence centered at about 45° latitude. For this wind distribution wavenumber 2 has an e -folding time of 3.0 days and a period of 6.3 days, as compared to 3.6 days and 17 days in the nondivergent case. The nondivergent model also predicted no growth for wavenumber 1, whereas the baroclinic 3-D model produced an e -folding time of 7.8 days and a period of 17 days for wavenumber 1 for the wind cross-section given in Fig. 12. The more rapid eastward progression of the unstable low wavenumber modes in the baroclinic model suggests the importance of divergence for these modes. In mid-latitudes the planetary vorticity gradient is substantial and nondivergent neutral modes of planetary scale tend to retrogress rapidly.

The effect of increasing vertical shear is shown in Table 5, where the growth rates and phase speeds for the first 4 wavenumbers are shown for shear profiles with $A = 75$ and $A = 50$. The sharper ($A = 50$) jet structure gives reduced growth rates at all wavenumbers, again consistent with Pfister's (1979) conclusions. Note that in this case the maximum growth rate occurs for wavenumber 3, which is consistent with the results from the nondivergent model shown in Table 3. The structure of wavenumber 3 growing on the shear zone wind distribution with $A = 75$ is shown in Fig. 15. The structure of this mode is similar to that for wavenumbers 1 and 2 except that wavenumber 3 does not propagate upward away from the jet level as well as the lower wavenumbers, and its amplitude distribution appears more elongated in the vertical than the lower wavenumbers. In the cases shown wavenumbers 1-3 all have geopotential height amplitude maxima near the top of the model. Stronger easterly shears above the jet maximum (not shown) tend to confine the waves closer to the level of excitation at the jet core. The growth rates and structure do not change much if the upper boundary is moved higher.

5. Discussion

The observations of high frequency eastward moving waves and of regions of negative potential vor-

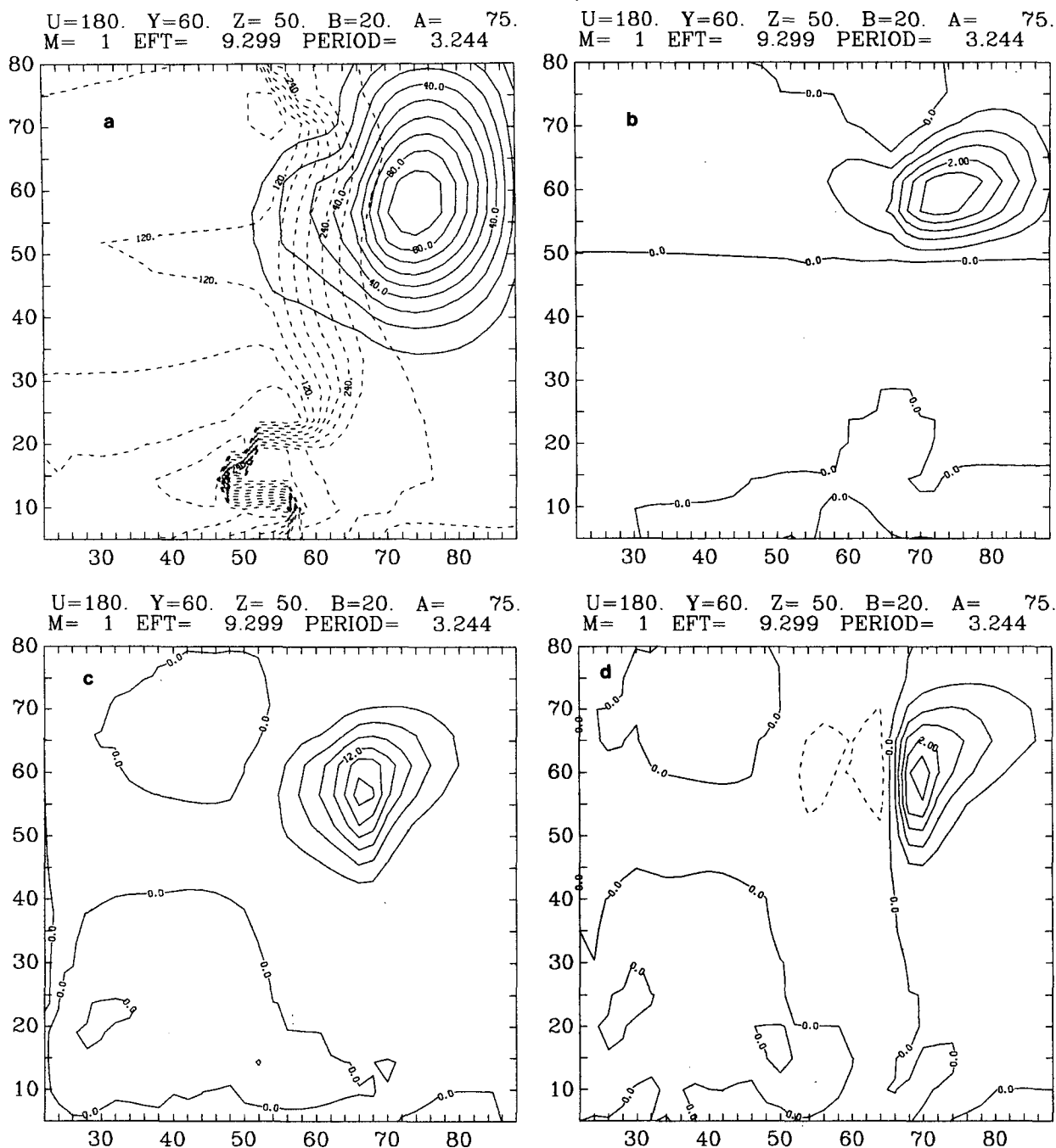
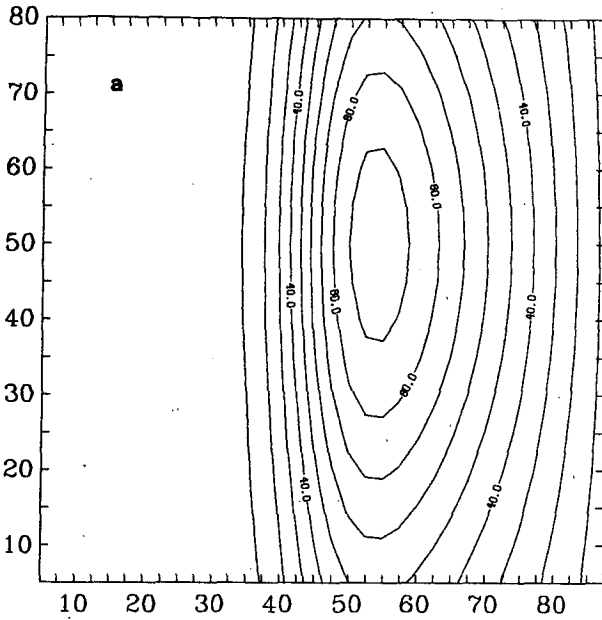


FIG. 12. Height versus latitude contour plots of (a) geopotential height amplitude (contour interval 10 m) and phase (contour interval 30° , positive to the east), (b) poleward eddy heat flux (contour interval 0.5 K m s^{-1}), (c) poleward eddy momentum flux (contour interval $3 \text{ m}^2 \text{ s}^{-2}$), (d) E-P flux divergence divided by cosine of latitude (contour interval $0.5 \text{ m s}^{-1} \text{ day}^{-1}$) for the unstable mode of zonal wavenumber 1 growing on the wind profile given in Fig. 11. Negative contours are dashed.

ticity gradient in the wintertime stratosphere have motivated an investigation of the barotropic instability of zonal mean wind distributions resembling those observed. In contrast to many past studies, spherical coordinates and terrestrial dimensions have been retained to facilitate comparison with observation. Eigenvalue solutions to the nondivergent vor-

ticity equation have been used to survey the dependence of unstable modes on the horizontal structure of the zonal mean wind. The influences of divergence and vertical shear on the most unstable modes for realistic but synthetic wind distributions were investigated using a time integration of a quasi-geostrophic model.

U=180. Y=45. Z= 50. B= 8. A= 75.



U=180. Y=45. Z= 50. B= 8. A= 75.

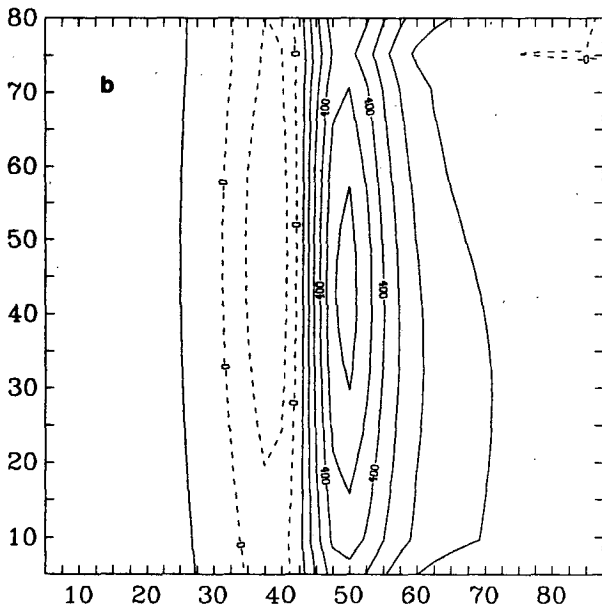


FIG. 13. As in Fig. 11 except for the shear zone wind distribution given by (11), with $\phi_0 = 45$, $B = 8$.

The barotropically unstable modes expected in association with a wind distribution like that of the polar-night jet stream can be divided into two classes. These two classes, which we have called polar modes and mid-latitude modes, are associated with regions of reversed potential vorticity gradient on the polar and mid-latitude flanks of the polar night jet stream. The most unstable polar mode for zonal wave-

number 1 has all of the properties of the so-called "4-day wave" described by Venne and Stanford (1982). For a realistic wind profile it has a period of 3.2 days and a maximum amplitude at about 70° latitude. The amplitude increases rapidly with height up to the level of the jet, and decreases above the jet if there are significant easterly shears there. The one potential disagreement between the model results and the observations of VS involves the latitudinal phase variations of the wave. VS obtained conflicting results for the phase variation in the Northern and Southern Hemispheres. In the Northern Hemisphere the wave was transporting momentum out of the jet, which is consistent with the model results and with the notion that the wave is a result of barotropic instability. In the Southern Hemisphere, where the wave is actually more pronounced, the momentum transport was found to be into the jet, suggesting barotropic stabilization of the wave. If this latter observation is borne out by further studies, then a source of excitation other than barotropic instability of the zonal mean state may be needed for the 4-day wave in the Southern Hemisphere.

An important simplification made in the present paper is the assumption of a mean state which is independent of longitude. Matsuno and Hirota (1966) and Hirota (1967) showed that longitudinally varying flows may be barotropically unstable, even when their zonal average is stable. When nondivergent mean state velocities $\bar{u}(x, y)$, $\bar{v}(x, y)$ are functions of both horizontal coordinates, then the energy equation for nondivergent perturbations on this state can be written (Hirota, 1967):

$$\frac{\partial}{\partial t} \left[\frac{1}{2} (\overline{u^2 + v^2}) \right] = - \left[\overline{u^2 \frac{\partial \bar{u}}{\partial x}} + \overline{v^2 \frac{\partial \bar{v}}{\partial y}} + \overline{u'v' \left(\frac{\partial \bar{u}}{\partial y} + \frac{\partial \bar{v}}{\partial x} \right)} \right] \quad (12)$$

where the overbar indicates an average over the domain. As indicated by (12), when the mean state depends on longitude it is not necessary for the zonally averaged perturbation momentum transport to be down the gradient of zonal-mean wind in order to transfer kinetic energy from the mean state to the perturbation. Triple products made up of two perturbation velocity components and both zonal and meridional gradients in the mean state velocities can produce wave growth even when $\overline{u'v'} = 0$. Longitudinal variations of the mean state may thus provide an explanation of why the meridional phase variation of the observed 4-day wave is weak and apparently variable. Another possible explanation of the observed phase shifts is that the polar mode exhibits the phase shift associated with barotropic instability only during its growth phase, has no phase shift when it attains maximum amplitude, and then switches to a phase shift consistent with barotropic stability during

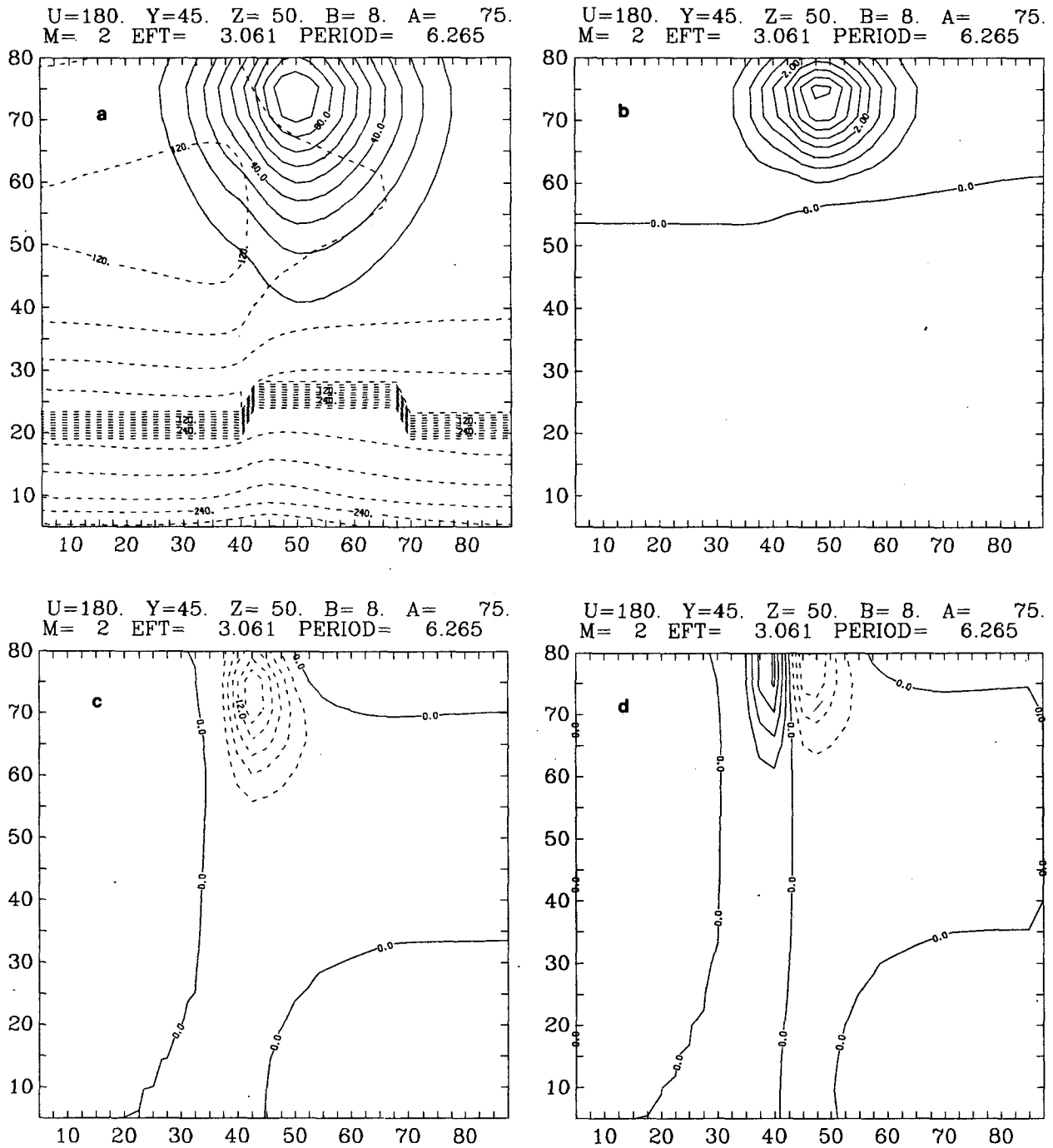


FIG. 14. As in Fig. 12 except for wavenumber 2 growing on the wind distribution shown in Fig. 13.

its decay phase. An amplitude weighted measure of phase averaged over such a life cycle might show very little shift with latitude. This seems even more likely when one considers that the vorticity gradient probably also varies in time. If the momentum flux and the sign of the vorticity gradient both vary in time, it is possible to obtain a net time-averaged barotropic eddy energy generation with time-averaged eddy momentum transport which is zero.

The asymmetries of the time-mean state in the Southern Hemisphere stratosphere are generally weak (e.g., see Hartmann, 1977) so that one would expect a zonally symmetric basic state to give a good first approximation. The results of Hirota (1967) and Frederiksen (1982) suggest that the addition of a small asymmetry to the flow would tend to increase the growth rate and the period of the unstable disturbances. These changes, together with a reduced re-

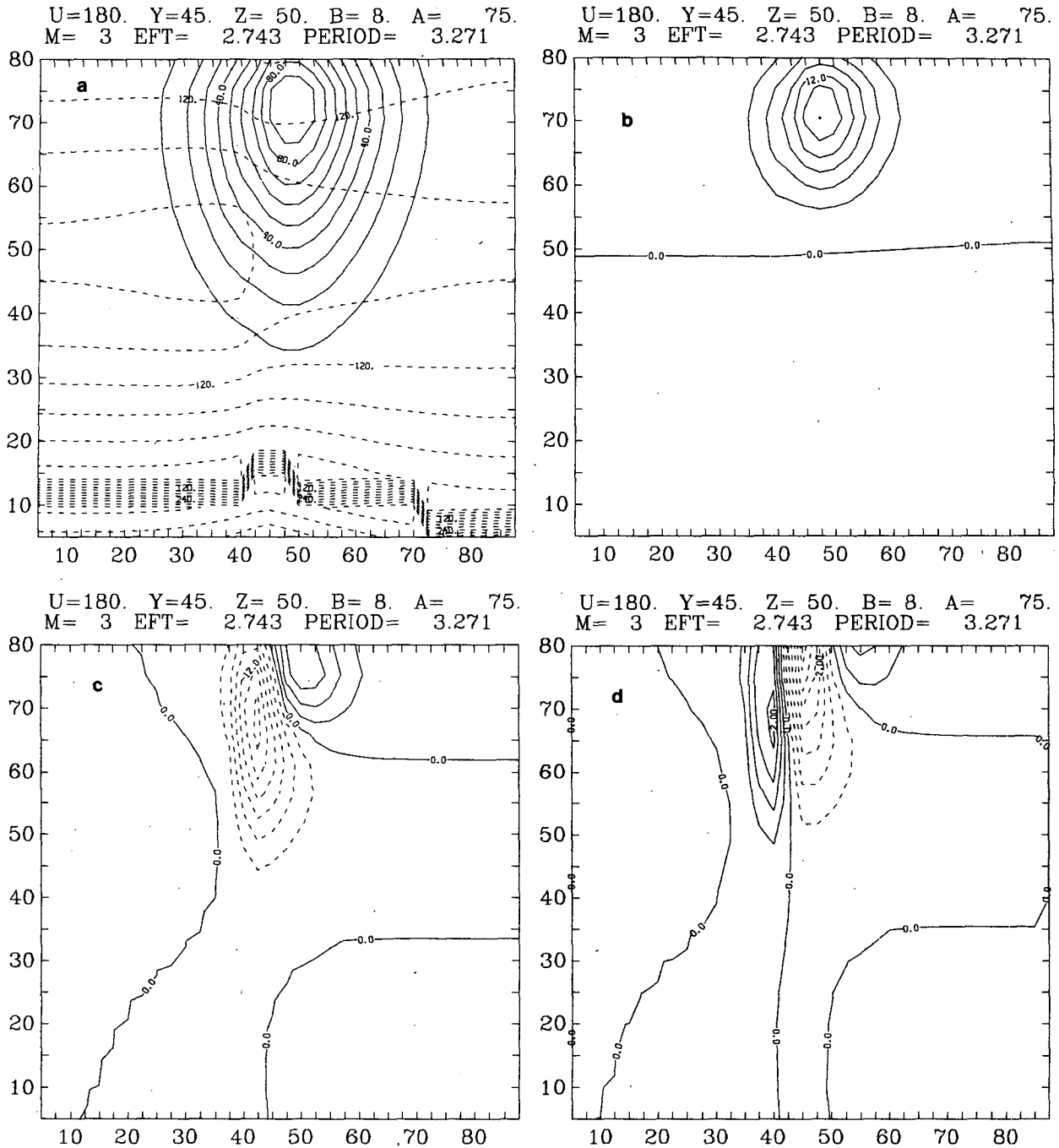


FIG. 15. As in Fig. 12 except for wavenumber 3 growing on the wind distribution given in Fig. 13. The contour interval for heat flux has been changed to 3 K m s^{-1} .

quirement for a specific meridional phase shift, would improve the agreement with observation, which is already good.

Along these same lines it is possible to argue that the presence of a 4-day period wavenumber 1 like that described here would enhance the growth rates of higher zonal wavenumbers. For the zonally symmetric basic state, the polar modes of zonal wavenumbers 1 and 2 have periods of roughly 3.0 and 1.6

days, respectively, so that their phase speeds are roughly equal. Frederiksen (1982) obtained maximum growth rates for perturbations which were stationary relative to the waves in the zonally asymmetric mean state. The presence of a wavenumber 1 4-day wave growing on a symmetric or slightly asymmetric basic state can thus be expected to favor the growth of higher wavenumbers moving along with the same phase speed. Apparently coherent relation-

TABLE 5. The e -folding times τ_i and periods τ_r obtained with the quasi-geostrophic baroclinic model for a shear zone wind profile given by (9) with $U = 180 \text{ m s}^{-1}$, $\phi_0 = 45^\circ$, $B = 8^\circ$, $Z_0 = 50 \text{ km}$, and two values of A .

A	Wavenumber							
	1		2		3		4	
	τ_i	τ_r	τ_i	τ_r	τ_i	τ_r	τ_i	τ_r
75	7.8	17	3.0	6.3	2.7	3.3	—	—
50	13	20	5.6	6.1	3.3	3.3	—	—

ships between eastward moving wavenumbers in the polar region have been observed by A. J. Prata (private communication, 1982).

The mid-latitude modes are associated with negative potential vorticity gradients which occur in the 30 to 40° latitude range. These modes have amplitude maxima near the latitude of maximum wind and rather broad meridional scales. Their energy generation arises from an equatorward momentum flux near the edge of the region of reversed potential vorticity gradient. For wind distributions which are near neutral stability the maximum growth rates occur for planetary wavenumbers 1–3. The periods for unstable mid-latitude modes of wavenumbers 1 and 2 are of the order of 3 weeks and 1 week respectively. Since these periods are near the time scales of the variations of wave forcing from the troposphere, we might expect important interactions between waves propagating upward from the troposphere and the instability of the polar night jet stream. This is particularly likely since the horizontal structure of the unstable modes is so similar to that of upward propagating waves. Because the growth rates for wavenumbers 1–3 are of the same order, it is likely that the zonal wavenumber with the largest initial amplitude, rather than the wave with the fastest growth rate, will derive the most energy from a region of reversed potential vorticity gradient. It is conceivable that in a highly time dependent mean flow with forced waves always present, the most unstable mode would never rise above the noise level, and it would be difficult to isolate the effect of the region of reversed potential vorticity gradient. One might expect to see, however, anomalously weak negative or even positive E–P flux divergences in a region of reversed zonal-mean potential vorticity gradient. Recently, Mechoso and Hartmann (1982) have shown that eastward moving planetary waves in the Southern Hemisphere stratosphere tend to be incoherent with their counterparts in the troposphere. Barotropic instability in the stratosphere could be an explanation of this behavior.

Acknowledgments. I would like to thank C. R. Mechoso and T. N. Palmer for discussions which motivated this study. D. A. Andrews, J. S. Frederiksen, C. B. Leovy, and an anonymous reviewer contributed useful criticisms of the original text. A. J. Prata and D. E. Venne provided interesting com-

munications on the observational aspects of the polar modes. Alan Bostick and Kay Moore helped prepare the manuscript. This work was supported by the Climate Dynamics Program, Climate Dynamics Research Section, Atmospheric Sciences Division, National Science Foundation under Grant ATM 81-06099.

REFERENCES

- Boyd, J. P., 1982: The influence of meridional shear on planetary waves. Part I: Nonsingular wind profiles. *J. Atmos. Sci.*, **39**, 756–769.
- Dickinson, R. E., and F. J. Clare, 1973: Numerical study of the unstable modes of a hyperbolic-tangent barotropic shear flow. *J. Atmos. Sci.*, **30**, 1035–1049.
- Edmon, H. J., Jr., B. J. Hoskins and M. E. McIntyre, 1980: Eliassen–Palm cross-sections for the troposphere. *J. Atmos. Sci.*, **37**, 2600–2616. [See also *Corrigendum*, *J. Atmos. Sci.*, **38**, 1115.]
- Frederiksen, J. S., 1982: Instability of the three-dimensional distorted polar vortex at the onset of the sudden warming. *J. Atmos. Sci.*, **39**, 2313–2329.
- Garcia, R. V., 1956: Barotropic waves in straight parallel flow with curved velocity profile. *Tellus*, **8**, 82–93.
- Hartmann, D. L., 1976: The structure of the stratosphere in the Southern Hemisphere during late winter 1973 as observed by satellite. *J. Atmos. Sci.*, **33**, 1141–1154.
- , 1977: Stationary planetary waves in the Southern Hemisphere. *J. Geophys. Res.*, **82**, 4930–4934.
- , 1979: Baroclinic instability of realistic zonal-mean states to planetary waves. *J. Atmos. Sci.*, **36**, 2336–2349.
- Hirota, I., 1967: Dynamic instability of the stratosphere polar vortex. *J. Meteor. Soc. Japan*, **45**, 409–421.
- Howard, L. N., and P. Drazin, 1964: On instability of parallel flow of inviscid fluid in a rotating system with variable Coriolis parameter. *J. Math. Phys.*, **43**, 83–99.
- Kuo, H. L., 1949: Dynamic instability of two-dimensional non-divergent flow in a barotropic atmosphere. *J. Meteor.*, **6**, 105–122.
- , 1973: Dynamics of quasi-geostrophic flows and instability theory. *Advances in Applied Mechanics*, **13**, Academic Press, 247–330.
- Leovy, C. B., 1964: Radiative equilibrium in the mesosphere. *J. Atmos. Sci.*, **21**, 238–248.
- , and T. Ackerman, 1973: Evidence for high-frequency synoptic disturbances near the stratopause. *J. Atmos. Sci.*, **30**, 940–942.
- , and P. J. Webster, 1976: Stratospheric long waves: Comparison of thermal structure in the Northern and Southern Hemispheres. *J. Atmos. Sci.*, **33**, 1624–1638.
- Lindzen, R. S., and K. K. Tung, 1978: Wave overreflection and shear instability. *J. Atmos. Sci.*, **35**, 1626–1632.
- Matsuno, T., and I. Hirota, 1966: On the dynamical stability of the polar vortex in wintertime. *J. Meteor. Soc. Japan*, **44**, 122–128.
- Mechoso, C. R., and D. L. Hartmann, 1982: An observational study of traveling planetary waves in the Southern Hemisphere. *J. Atmos. Sci.*, **39**, 1921–1935.
- Michalke, A., 1964: On the inviscid instability of the hyperbolic tangent velocity profile. *J. Fluid Mech.*, **19**, 543–556.
- Pfister, L., 1979: A theoretical study of three-dimensional barotropic instability with applications to the upper stratosphere. *J. Atmos. Sci.*, **36**, 908–920.
- Tung, K. K., 1981: Barotropic instability of zonal flows. *J. Atmos. Sci.*, **38**, 308–321.
- Venne, D. E. and J. L. Stanford, 1982: An observational study of high-latitude stratospheric planetary waves in winter. *J. Atmos. Sci.*, **39**, 1026–1034.
- , and —, 1979: Observation of a 4-day temperature wave in the polar winter stratosphere. *J. Atmos. Sci.*, **36**, 2016–2019.